Check for updates

CHEMISTRY

Hyperselective carbon membranes for precise high-temperature H_2 and CO_2 separation

Gaurav M. Iyer, Ching-En Ku, Chen Zhang*

Copyright © 2025 The Authors, some rights reserved; exclusive licensee American Association for the Advancement of Science. No claim to original U.S. Government Works. Distributed under a Creative Commons Attribution NonCommercial License 4.0 (CC BY-NC).

More than 90% of the world's hydrogen (H_2) is produced from fossil fuel sources, which requires energy-intensive separation and purification to produce high-purity H_2 fuel and to capture the carbon dioxide (CO_2) by-product. While membranes can decarbonize H_2/CO_2 separation, their moderate H_2/CO_2 selectivity requires secondary H_2 purification by pressure swing adsorption. Here, we report hyperselective carbon molecular sieve hollow fiber membranes showing H_2/CO_2 selectivity exceeding 7000 under mixture permeation at 150°C, which is almost 30 times higher than the most selective nonmetallic membrane reported in the literature. The membrane is able to maintain an ultrahigh H_2/CO_2 selectivity over 1400 under mixture permeation at 400°C. Pore structure characterization suggests that highly refined ultramicropores are responsible for effectively discriminating the closely sized H_2 and CO_2 molecules in the hyperselective carbon molecular sieve membrane. Modeling shows that the unprecedented H_2/CO_2 selectivity will potentially allow one-step enrichment of fuel-grade H_2 from shifted syngas for decarbonized H_2 production.

INTRODUCTION

Hydrogen (H_2) is a clean and efficient fuel for power generation and transportation owing to its zero-emission combustion and high energy density. While water electrolysis and other nonthermal routes have gained momentum in recent years, fossil fuel–based methods still dominate H_2 production. In the US, 95% of H_2 is produced from natural gas reforming (*1*), in which methane (CH_4) is reacted with steam to produce syngas comprising H_2, carbon monoxide (CO), and a small amount of carbon dioxide (CO_2). The syngas is then sent through a series of high-temperature (up to 450°C) and low-temperature (up to 250°C) water-gas shift (WGS) reactors to increase the H_2 yield and convert the harmful CO to CO_2. The shifted syngas leaving the low-temperature WGS reactor is at up to 250°C and 15 bar containing H_2, CO_2, unreacted CH_4, and a trace amount of CO (*2*). Enrichment of the H_2 product and capture of CO_2 from shifted syngas are commercially practiced by pressure swing adsorption or less commonly by cryogenic distillation. The separations rely on either electrical or thermal energy and are energy intensive to produce high-purity H_2 product that can meet the purity requirements for power generation fuel (>99.9%) or fuel cell vehicle (>99.97%) applications (*3*). The US produces 10 million tons of H_2 every year by natural gas reforming (*4*), and more energy-efficient H_2 enrichment technologies can contribute to the decarbonization of H_2 production.

Membranes can take advantage of the high pressure of shifted syngas to achieve H_2/CO_2 separation without the input of thermal or electrical energy and are therefore more energy efficient than pressure swing adsorption or distillation. Palladium and its alloy membranes can give theoretically infinite H_2/CO_2 selectivity by the H_2 dissociation-reassociation mechanism. Nevertheless, applying these metallic membranes for large-scale separations has been challenged by membrane cost, contamination by impurities (e.g., H_2S and CO), and H_2 embrittlement (*2*). Nonmetallic membranes based on the sorption-diffusion mechanism are already commercialized for air separation and natural gas purification (*5*, *6*). However, H_2/CO_2 separation is known as one of the most challenging gas separations for sorption-diffusion membranes. While diffusion favors H_2 with slightly smaller kinetic diameter (H_2: 2.89 Å versus CO_2: 3.3 Å), sorption favors the more condensable CO_2 with much higher critical temperature (H_2: −240°C versus CO_2: 31°C) (*7*). Carbon molecular sieve (CMS) membranes are promising nonmetallic membranes for H_2 enrichment from shifted syngas owing to their outstanding permeability and selectivity under high-temperature (*8*) and high-pressure (*9*) conditions. CMS membranes are made by pyrolysis of polymer precursors and consist of ultramicropore slits governing membrane selectivity (*10*–*13*). They can be made into commercially proven hollow fibers with thin separation layers and high permeance (*14*). CMS membranes have shown the highest H_2/CO_2 selectivity (~260) among nonmetallic membranes under shifted syngas conditions (*15*). Such a selectivity, however, is still not high enough for one-step enrichment of fuel-grade H_2. Additional purification must be used, which compromises the attractiveness of membrane separation. Because of limited membrane selectivity, most published research on membrane-based H_2/CO_2 separation has been geared toward CO_2 capture (*16*) from H_2 production rather than high-purity H_2 production. One-step enrichment of fuel-grade H_2 requires hyperselective membranes under aggressive shifted syngas conditions. Here, we report unprecedented H_2/CO_2 selectivity exceeding 7000 in aromatic polyamide (aramid)–derived CMS hollow fiber membranes under shifted syngas conditions. Modeling suggests that these hyperselective CMS hollow fiber membranes will potentially allow one-step enrichment of high-purity fuel-grade H_2.

RESULTS

H_2/CO_2 separation performance of CMS membranes

Aramid was synthesized by stirred interfacial polymerization of *m*-phenylenediamine and a mixture of terephthaloyl chloride and isophthaloyl chloride (*17*). Aramid hollow fibers (Fig. 1A) were fabricated by dry-jet/wet-quench spinning (table S1) and used as a precursor to fabricate aramid-derived CMS hollow fiber membranes (codenamed Aramid-1050; Fig. 1B) by pyrolysis at 1050°C

Department of Chemical and Biomolecular Engineering, University of Maryland, College Park, MD, 20742, USA.
*Corresponding author. Email: czhang71@umd.edu

Downloaded from https://www.science.org on August 28, 2026

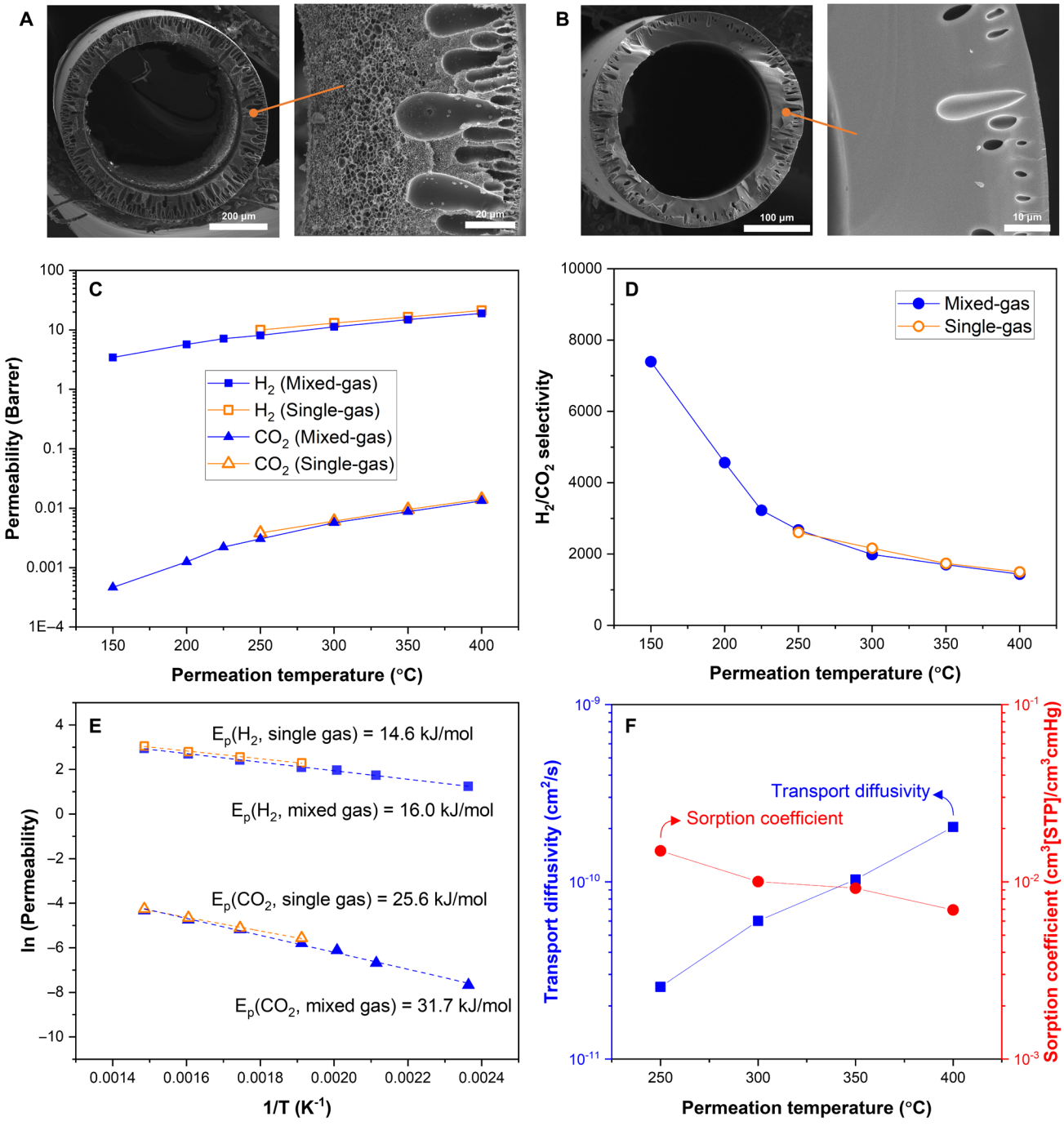


Fig. 1. H_2/CO_2 separation performance of the Aramid-1050 CMS membrane. Scanning electron microscopy images of (**A**) the aramid precursor hollow fiber and (**B**) Aramid-1050 CMS membrane. (**C**) Effect of permeation temperature on H_2 permeability and H_2/CO_2 selectivity. (**D**) Effect of permeation temperature on H_2/CO_2 selectivity. (**E**) Arrhenius plots of H_2 permeabilities and CO_2 permeabilities. (**F**) Effects of permeation temperature on CO_2 transport diffusivity and sorption coefficient. Mixed-gas permeation was measured using a 10% H_2/90% CO_2 mixture at 2 bar.

for 2 hours. The aramid hollow fibers had an outer diameter around 715 µm and contained macrovoids. After pyrolysis, the CMS hollow fiber outer diameter was reduced to roughly 323 µm and some macrovoids were retained. Because no macrovoids were seen to run through the CMS hollow fiber wall, it was believed that they did not cause membrane defects or negatively affect membrane selectivity, which was confirmed by permeation (Fig. 1, C and D). The Aramid-1050 CMS membrane had an effective separation layer thickness of 41 µm, which was calculated from CMS hollow fiber wall thickness taking into account the volume fraction of macrovoids.

Mixture H_2/CO_2 permeation measurements were carried out at 150° to 400°C and a feed pressure of 2 bar (Fig. 1, C and D). While a

Downloaded from https://www.science.org on August 28, 2026

50% H_2/50% CO_2 mixture feed is commonly used in the literature for H_2/CO_2 mixed-gas permeation studies, a 10% H_2/90% CO_2 mixture feed was predominantly used in this work because a higher feed CO_2 concentration allowed more reliable determination of permeate composition for the hyperselective membranes. Under 150°C permeation, the Aramid-1050 CMS membrane showed a H_2 permeability of 3.4 Barrer (1 Barrer = 10^{-10} cm^3[STP]·cm/cm^2·s·cmHg) and a H_2/CO_2 selectivity of 7395. To our best knowledge, this is the highest H_2/CO_2 selectivity measured in nonmetallic membranes based on the sorption-diffusion mechanism. As the permeation temperature increased to 400°C, H_2 permeability increased to 19 Barrer with a drop in H_2/CO_2 selectivity. Nevertheless, the membrane still showed an outstanding H_2/CO_2 selectivity of 1437 under 400°C permeation, which will be attractive to enhance CO conversion of WGS membrane reactors by selective H_2 removal (*18*, *19*).

In addition to mixed-gas H_2/CO_2 permeation, we carried out single-gas H_2 and CO_2 permeation (Fig. 1, C and D) in the Aramid-1050 CMS membrane at 250° to 400°C using the constant-volume method. Single-gas permeation below 250°C was not performed because of the small ratio between CO_2 permeation slope and leak rate. Prior CMS membrane work (*20*) showed both higher H_2 permeability and higher H_2/CO_2 selectivity in single-gas permeation than mixed-gas permeation at permeation temperatures below 150°C, which can be attributed to strong competitive sorption of CO_2 under mixed-gas permeation. The single-gas permeabilities in the Aramid-1050 CMS membrane were slightly higher at 250°C, and the difference became negligible as the permeation temperature reached 400°C. It is hypothesized that CO_2 sorption was suppressed as the permeation temperature increased, which reduced the competitive sorption effects. This hypothesis was supported by the fact that the feed H_2/CO_2 molar ratio had limited effects on H_2/CO_2 selectivity as feed H_2 concentration increased from 10 to 75% under 400°C permeation (table S2).

The Arrhenius plots of H_2 and CO_2 permeabilities measured from mixed-gas permeation and single-gas permeation are shown in Fig. 1E. The Arrhenius plots had good linearity, allowing the calculation of H_2 and CO_2 permeation activation energies. The permeation of CO_2 requires more activation energy than H_2 under both mixed-gas and single-gas permeation. Permeation activation energy is the summation of positive diffusion activation energy and negative heat of adsorption. The CO_2 heat of adsorption was likely larger than the H_2 heat of adsorption because of the higher condensability of CO_2. Thus, the larger CO_2 permeation activation energy was presumably due to its substantially larger diffusion activation energy, which can be attributed to the CMS membrane's highly refined and size-discriminating ultramicropores. The permeation activation energies for H_2 and CO_2 in mixed-gas permeation were higher compared to those in single-gas permeation possibly due to competition from the other permeation species, although the effect was not very pronounced. The good linearity of the Arrhenius plots allowed the prediction of H_2/CO_2 separation performance at a broader range of permeation temperatures. For example, the membrane has a predicted H_2/CO_2 mixed-gas selectivity exceeding 36,000 under 35°C permeation (fig. S1). Such an extraordinary selectivity, however, will be challenging to measure experimentally because of the long time required to reach steady-state permeation and the difficulty to analyze ultralow permeate CO_2 concentration.

The transport diffusivities of CO_2 at 250° to 400°C were calculated using the time-lag method from CO_2 permeation plots (fig. S2), which further allowed us to calculate CO_2 sorption coefficients based on the sorption-diffusion mechanism using measured single-gas CO_2 permeabilities (Fig. 1F). The reduction in CO_2 sorption coefficient supports our hypothesis that CO_2 sorption was suppressed at higher permeation temperatures. The Arrhenius plot of CO_2 transport diffusivities and van't Hoff plot of CO_2 sorption coefficients both showed good linearity (fig. S3), enabling the calculation of CO_2 diffusion activation energy (39.6 kJ/mol) and CO_2 heat of adsorption (−14 kJ/mol). Characterizing high-temperature diffusion and sorption in membrane and sorbent materials has been challenging and often relies on expensive commercial instruments. This work has shown that high-temperature diffusion and sorption can be studied using the constant-volume permeation method, which was traditionally only used at ambient temperature.

The Aramid-1050 CMS membrane had outstanding robustness under long-term and high-pressure H_2/CO_2 mixture permeation (Fig. 2). At 250°C, the membrane had stable H_2 permeability and H_2/CO_2 selectivity without physical aging for at least 2 weeks following a transient period of 5 days (Fig. 2A). Physical aging has been reported in CMS membranes as a result of the membrane pore structure approaching a thermodynamically stable state, which gave reduced permeability and increased selectivity over time (*21*). Physical aging is usually more pronounced in CMS membranes with open pore structures pyrolyzed at lower pyrolysis temperatures. The Aramid-1050 CMS membrane showed no physical aging, possibly because the high pyrolysis temperature gave the membrane a highly refined pore structure that was already at a relatively thermodynamically stable state. The Aramid-1050 CMS membrane was also able to maintain its highly attractive separation performance under elevated pressure. As the H_2/CO_2 mixture feed pressure increased from 2 to 15 bar, the membrane showed a negligible change in H_2 permeability and H_2/CO_2 selectivity (Fig. 2B). This finding is consistent with a previous work (*9*) that CMS membranes can maintain attractive selectivity under high-pressure condensable feeds. The H_2/CO_2 separation performance of the Aramid-1050 CMS membrane was compared with other nonmetallic membranes reported in the literature (Fig. 2C and table S2) measured using H_2/CO_2 mixture feed at permeation temperature above 100°C, which include zeolite membranes, metal-organic framework membranes, covalent-organic framework membranes, porous-organic framework membranes, silica membranes, graphene oxide membranes, and other CMS membranes (*15*, *20*, *22*–*24*). The Aramid-1050 CMS membrane showed almost 30 times higher H_2/CO_2 selectivity than the most selective nonmetallic membrane reported in the literature, which is a ladder polymer (CANAL)–derived CMS membrane (*15*). It is worthwhile to note that a graphene oxide membrane (*25*) can provide ultrahigh H_2/CO_2 selectivity exceeding 3000 at room temperature, which dropped to 250 at 100°C.

Understanding the unprecedented H_2/CO_2 selectivity

Comparing with the Aramid-925 CMS membrane (*17*) pyrolyzed at a lower temperature (925°C) allowed an understanding of the unprecedented H_2/CO_2 selectivity in the Aramid-1050 CMS membrane. The Aramid-925 CMS membrane has a H_2 permeability of 20.7 Barrer and a H_2/CO_2 selectivity of 200 under 150°C permeation (fig. S4). The higher selectivity and lower permeability in the Aramid-1050 CMS membrane were likely due to its more refined ultramicropores formed at higher pyrolysis temperature, which is consistent with observations in polyimide-derived CMS membranes (*26*). A trade-off in H_2 permeability and H_2/CO_2 selectivity is seen as the CMS membrane pyrolysis temperature increases (fig. S5). While even higher

Downloaded from https://www.science.org on August 28, 2026

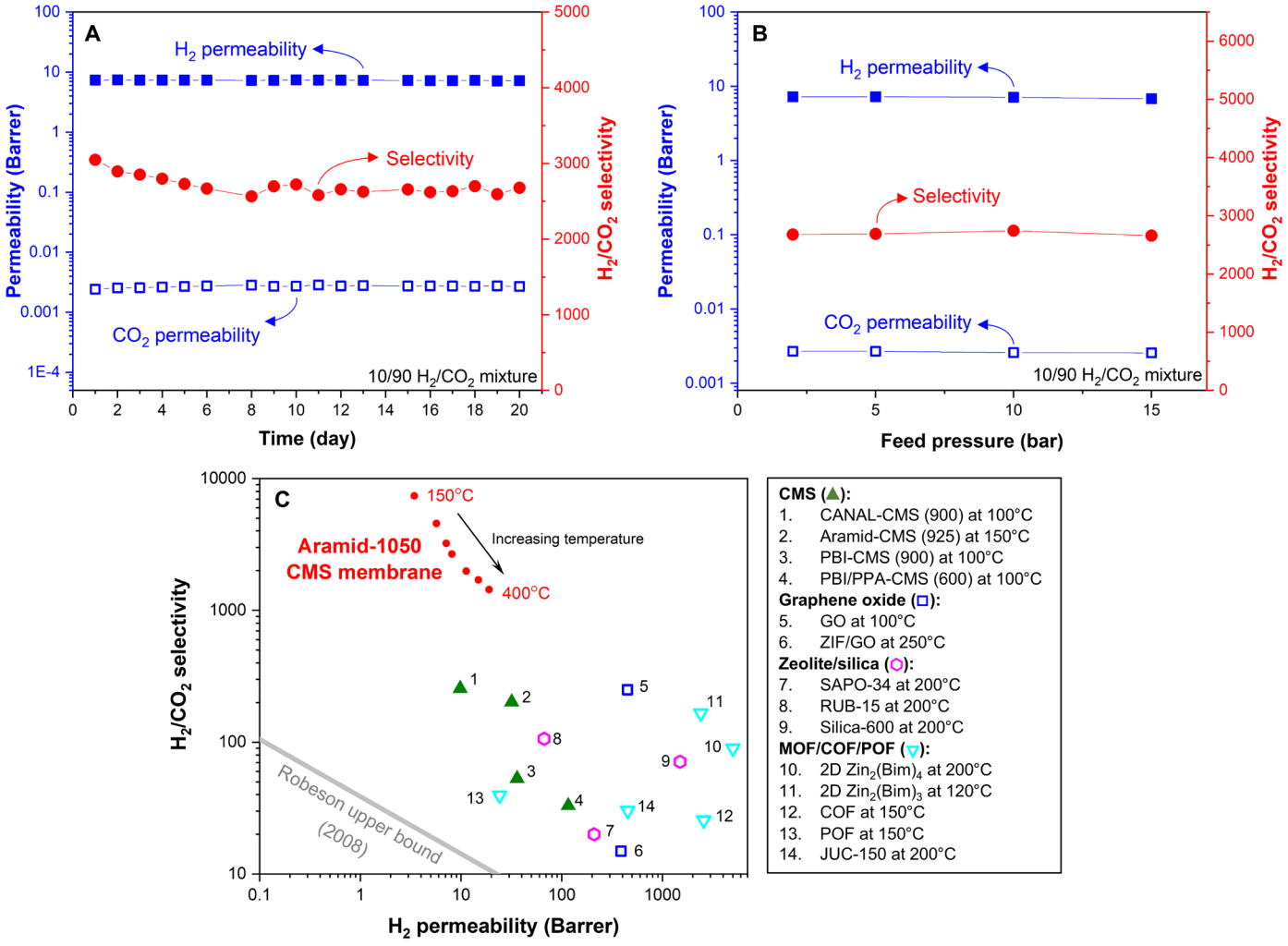


Fig. 2. Robustness and competitiveness of the Aramid-1050 CMS membrane for H_2/CO_2 separation. (**A**) Long-term stability of H_2 permeability and H_2/CO_2 selectivity in the Aramid-1050 CMS membrane. Permeation was carried out at 250°C and a feed pressure of 2 bar. (**B**) Effect of feed pressure on H_2 permeability and H_2/CO_2 selectivity in the Aramid-1050 CMS membrane. Permeation was carried out at 250°C. (**C**) Comparing the mixed-gas separation performance of the Aramid-1050 CMS membrane with other nonmetallic membranes reported in the literature (permeation temperature above 100°C).

H_2/CO_2 selectivity can be expected in the CMS membrane if the pyrolysis temperature is further increased above 1050°C, H_2 permeability will likely be even lower.

Unlike the Aramid-1050 CMS membrane, the H_2/CO_2 selectivity of the Aramid-925 CMS membrane increased with permeation temperature (fig. S4), showing smaller CO_2 permeation activation energy than H_2 permeation activation energy (Fig. 3A). The Aramid-1050 CMS membrane had slightly higher H_2 permeation activation energy (15.8 versus 13.2 kJ/mol) and substantially higher CO_2 activation energy (34 versus 8.8 kJ/mol) than the Aramid-925 CMS membrane. Because both CMS membranes have relatively nonpolar surfaces with negligible functional groups, it can be assumed that the two membranes have very comparable heats of adsorption. Hence, the higher permeation activation energies in the Aramid-1050 CMS membrane can be attributed to higher diffusion activation energies, which is evidence that the Aramid-1050 CMS membrane has more refined ultramicropores. The increase in CO_2 diffusion activation energy was more pronounced because it has larger kinetic diameter than H_2 and is therefore more sensitive to changes in ultramicropore size. The two CMS membranes showed almost identical H_2 sorption capacity (Fig. 3B). However, the refined ultramicropores substantially reduced CO_2 sorption capacity in the Aramid-1050 CMS membrane by exclusion of the larger CO_2 molecules. Such exclusion possibly reduced competition between H_2 and CO_2 in CMS membrane micropores under mixed-gas permeation, which contributed to the close mixed-gas and single-gas H_2/CO_2 selectivities seen in Fig. 1D.

The sp^3/sp^2 carbon ratio of the CMS membranes was determined by analyzing the high-resolution C1s spectra obtained from x-ray photoelectron spectroscopy (XPS) (Fig. 3C and fig. S6). The Aramid-1050 CMS membrane showed lower sp^3/sp^2 carbon ratio, suggesting a more ordered graphitic structure (*27*), thereby supporting the hypothesis that the Aramid-1050 CMS membrane had more refined ultramicropores. The XPS results were further corroborated by Raman spectroscopy (Fig. 3D). The Aramid-1050 CMS membrane showed a lower I_{D1}/I_G ratio, indicating higher concentration of

Downloaded from https://www.science.org on August 28, 2026

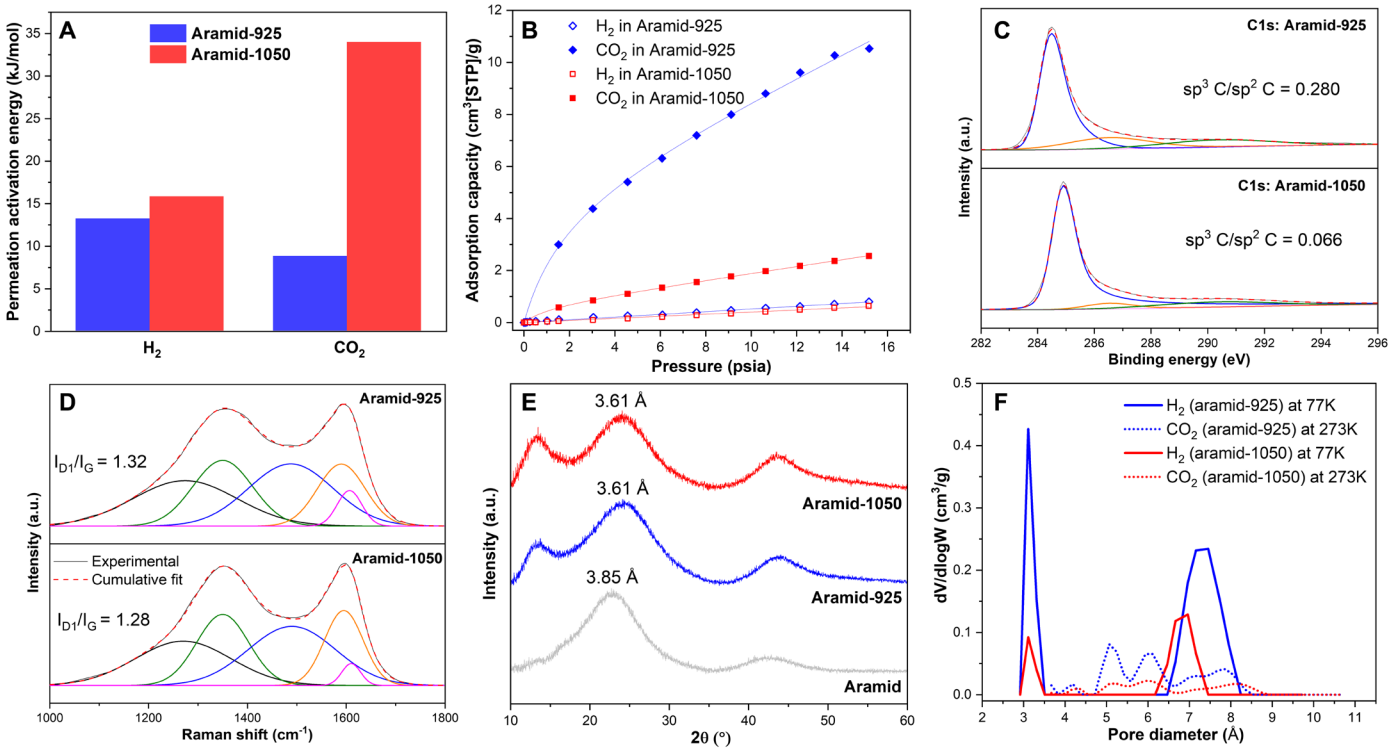


Fig. 3. Understanding the unprecedented selectivity in the Aramid-1050 CMS membrane. (**A**) H_2 and CO_2 permeation activation energies in the Aramid-1050 CMS membrane and Aramid-925 CMS membrane. (**B**) H_2 and CO_2 equilibrium sorption isotherms at 35°C. (**C**) High-resolution C1s spectra of CMS membranes. a.u., arbitrary units. (**D**) Raman spectra of CMS membranes. (**E**) WAXD patterns of the aramid precursor and CMS membranes showing average d-spacing. (**F**) Pore size distribution curves of the CMS membranes calculated using CO_2 physisorption (273.15 K) and H_2 physisorption (77 K) isotherms using the density functional theory.

sp^2 carbon (*11*). Wide-angle x-ray diffraction (WAXD; Fig. 3E) suggested that the Aramid-1050 and Aramid-925 CMS membranes had almost identical d-spacing (3.61 Å), which were both smaller than the aramid precursor (3.85 Å). Several recent studies (*22*, *26*) show that WAXD had limitations to characterize highly refined CMS ultramicropores.

Physisorption of CO_2 at 273.15 K is often used to measure CMS membrane pores larger than 3.3 Å (*26*). Because of CO_2 exclusion by the highly refined ultramicropores, both the Aramid-925 and Aramid-1050 CMS membranes showed low pore volume and surface area calculated from CO_2 physisorption isotherms at 273.15 K (Fig. 3F and fig. S7). We found that cryogenic H_2 physisorption at 77 K was more useful to characterize the pore structure of aramid-derived CMS membranes. Because of its smaller kinetic diameter, H_2 was able to access pores as small as 3 Å. The pore size distribution obtained from H_2 physisorption shows a primary peak around 3 to 4 Å and a secondary peak around 6 to 8 Å. The Aramid-1050 CMS membrane had a shorter primary peak and smaller pore volume, indicating its more compact pore structure and more effective exclusion of CO_2 (3.3 Å). Physisorption of H_2 at 77 K has been reported to measure the pore size of activated carbon but not CMS membranes (*28*).

Modeling of membrane separators for one-step H_2 enrichment

The unprecedented H_2/CO_2 selectivity of the Aramid-1050 CMS membrane opens up H_2 separation opportunities that were previously unattainable with nonmetallic membranes. Commercially proven membrane-based gas separations often rely on the enrichment of the slower-permeating gas of a mixture in the retentate stream. For example, 99% N_2 can be enriched in the retentate stream of membrane air separators using moderately selective {$\alpha[O_2/N_2] < 7$} polymer membranes. Enrichment of high-purity gas in the permeate stream is more challenging, and it is often argued that permeate purity can be limited by pressure ratio, i.e., the ratio of feed and permeate pressures (*29*). Shifted syngas usually consists of 50 to 80% H_2 (*2*). Hence, enrichment of high-purity H_2 from shifted syngas is not limited by pressure ratio and can be enabled by hyperselective membranes. A one-dimensional isothermal model was used to simulate an Aramid-1050 CMS membrane separator (Fig. 4A) that enriches H_2 (in the permeate stream) and captures CO_2 (in the retentate stream) from shifted syngas feed at 150°C and 15 bar. The results were compared with the Aramid-925 CMS membrane with a H_2/CO_2 selectivity of 200 and the polybenzimidazole (PBI) polymer membrane with a H_2/CO_2 selectivity of 15, which represents the state-of-the-art polymer membrane (*30*) reported in the literature. The shifted syngas feed (table S3) consisted of 74.1% H_2, 18.5% CO_2, 6.9% CH_4, and 0.5% CO (*2*). It was assumed that the Aramid-1050 CMS membrane was impermeable to CH_4 and CO, considering their much larger kinetic diameter (both ~3.8 Å) than CO_2. While shifted syngas feed contains water vapor, previous studies (*20*, *23*) found that feed water vapor had a negligible influence on CMS membrane H_2/CO_2 selectivity and limited effects on CMS membrane H_2 permeability. A membrane separation layer thickness of 41 μm (table S4) was assumed for all membranes

Downloaded from https://www.science.org on August 28, 2026

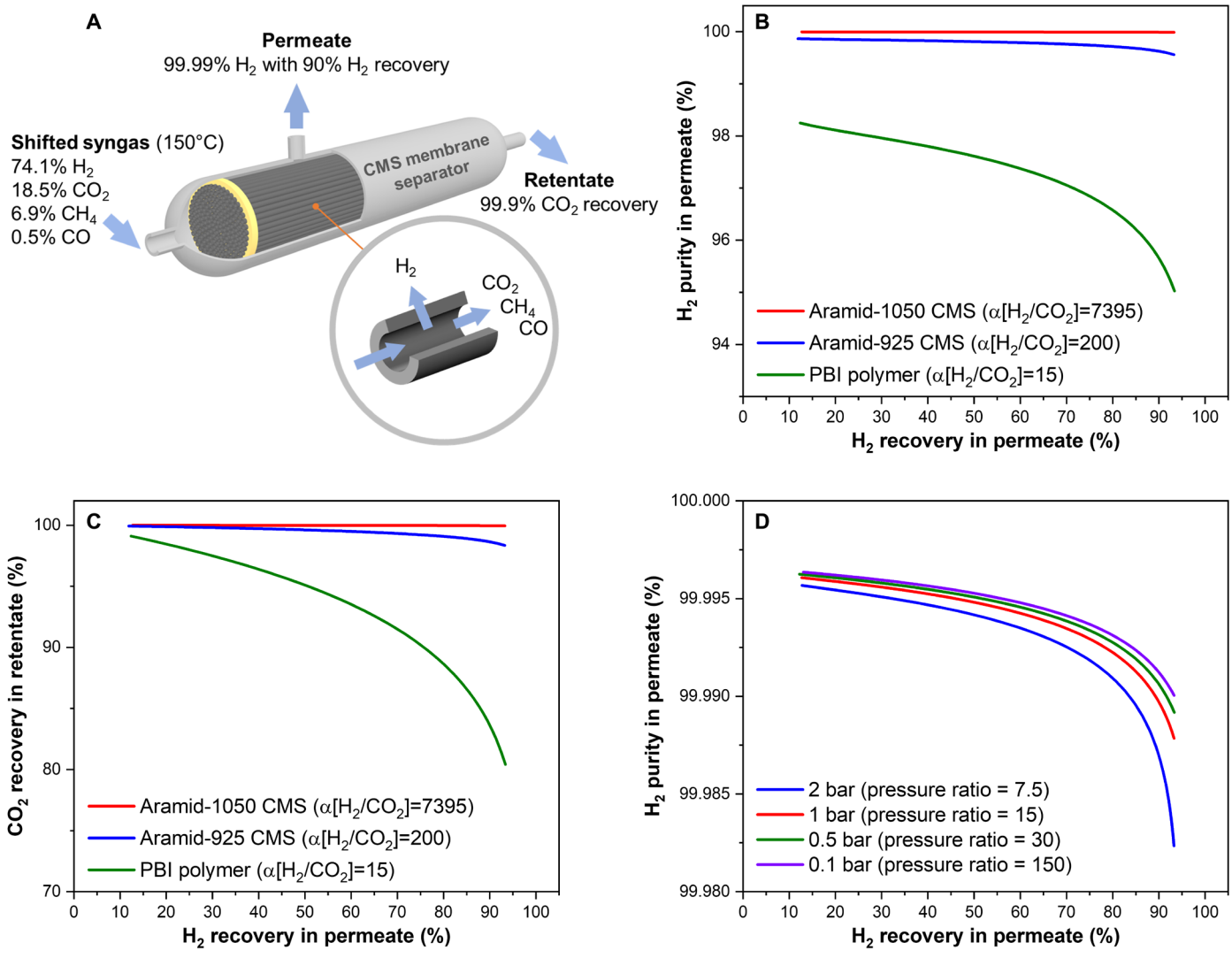


Fig. 4. Modeling of membrane separators for H_2 enrichment and CO_2 capture from shifted syngas. (**A**) Schematics illustrating the hyperselective CMS hollow fiber membrane separator for H_2/CO_2 separation. The effects of H_2 recovery on (**B**) permeate stream H_2 purity and (**C**) retentate stream CO_2 recovery in the Aramid-1050 CMS membrane, Aramid-925 CMS membrane, and polybenzimidazole (PBI) polymer membrane separators. (**D**) The effects of permeate stream pressure (and therefore pressure ratio) on permeate stream H_2 purity in the Aramid-1050 CMS membrane separator.

in the model. It should be noted that smaller membrane areas and reduced capital costs are expected as the membrane thickness is reduced and permeance is increased.

Commercial pressure swing adsorption units usually operate with ~90 to 95% H_2 recovery (*31*). The hyperselective Aramid-1050 CMS membrane separator can produce 99.99% pure H_2 (Fig. 4B) from shifted syngas feed with 90% H_2 recovery. Therefore, the membrane allows one-step enrichment of high-purity H_2 fuel without secondary purification, thereby simplifying the H_2 fuel production process. A more complex two-stage membrane separation system would further increase H_2 purity, however, with the added cost of interstage compression. The Aramid-1050 CMS membrane separator is also highly efficient to recover CO_2 from the shifted syngas feed with 99.9% CO_2 recovery in the retentate stream (Fig. 4C). A practical permeate pressure of 1 bar was used in the model (*32*). Therefore, the membrane separator is fully decarbonized because the separation is solely driven by the high pressure of shifted syngas without compression or vacuum. Permeate pressure (and, therefore, pressure ratio) had a limited influence on permeate stream H_2 purity (Fig. 4D) of the Aramid-1050 CMS membrane separator. As the permeate stream pressure increased from 0.1 to 2 bar, the permeate stream H_2 purity only dropped by 0.004% under the same 90% H_2 recovery. A trade-off in H_2 purity and process economics is seen for CMS membranes made at lower pyrolysis temperature. With much lower H_2/CO_2 selectivities, the Aramid-925 CMS membrane separator can only produce 99.6% pure H_2 under the same 90% H_2 recovery. However, because of the higher permeability and permeance of the Aramid-925 CMS membrane, smaller membrane areas (fig. S8) and presumably lower membrane costs are required to achieve the same H_2 recovery with the Aramid-1050 CMS membrane, assuming identical membrane separation layer thickness.

Downloaded from https://www.science.org on August 28, 2026

DISCUSSION

We report an ultrahigh H_2/CO_2 mixed-gas selectivity over 7000 at 150°C in hyperselective CMS membranes fabricated by pyrolysis of an aramid precursor. The H_2/CO_2 selectivity of the hyperselective CMS membrane was unprecedented and 30 times higher than the most selective nonmetallic membranes. The hyperselective CMS membrane was able to maintain an ultrahigh H_2/CO_2 mixed-gas selectivity over 1400 at 400°C, which was the highest temperature reported for CMS membranes for H_2/CO_2 separation. High-temperature diffusion and sorption analysis was carried out using single-gas permeation, which further validated the ultrahigh H_2/CO_2 separation performance. Contrary to previously reported CMS membranes, the hyperselective CMS membrane showed very close H_2/CO_2 selectivity in mixed-gas and single-gas permeation, which was attributed to partial CO_2 exclusion and suppressed CO_2 sorption at high permeation temperature. Pore structure characterization by a cryogenic H_2 physisorption method suggested that highly refined ultramicropores were responsible for effectively discriminating the closely sized H_2 and CO_2 molecules in the hyperselective CMS membrane. The material discovery reported in this work opens up H_2 separation opportunities that were previously unattainable with nonmetallic membranes based on the sorption-diffusion mechanism. Notably, modeling shows that a membrane separator consisting of the hyperselective CMS membrane can produce 99.99% fuel-grade H_2 from shifted syngas without secondary purification at H_2 recovery (90%) comparable with commercial pressure swing adsorption.

It should be noted that the unprecedented H_2/CO_2 selectivity of the Aramid-1050 CMS membrane was obtained with a compromise in H_2 permeability. The membrane made in this work had a thick separation layer and low H_2 permeance (fig. S9), requiring large membrane areas. Therefore, ultrathin defect-free composite membranes (*14*, *33*) must be made to provide improved permeance and therefore reduced membrane area (fig. S8) and separator capital cost, which is needed for the membrane process to be economically competitive with commercial pressure swing adsorption. Also, the modeling was done on the basis of membrane separation performance measured from binary H_2/CO_2 mixture permeation with low stage cut. Permeation using realistic shifted syngas feeds under higher stage cut will be needed to validate the modeling results. Although CMS hollow fiber membranes are more flexible than other inorganic membranes such as ceramic hollow fiber membranes, they are not as flexible as polymer hollow fiber membranes. Breakthroughs in scaling up CMS membranes must be made to enable their large-scale manufacture and application. This fact notwithstanding, the findings of this work demonstrate the possibility of decarbonized one-step enrichment of high-purity fuel-grade H_2 using nonmetallic membranes based on the sorption-diffusion mechanism.

MATERIALS AND METHODS

Fabrication of polymer precursor hollow fibers

The aramid precursor was synthesized by stirred interfacial polymerization following a procedure described elsewhere (*17*). Monolithic aramid precursor hollow fiber membranes were made from the synthesized aramid by the dry-jet/wet-quench spinning process using a customized hollow fiber spinning system (fig. S10) (*34*). Aramid powders were dried under vacuum at 110°C for 12 hours before preparing the spinning solution. The spinning solution composition and spinning conditions can be found in table S1. Tap water was used in the quench bath. The as-spun precursor hollow fibers were soaked in deionized water for 3 days, followed by soaking in methanol for 60 min and hexane for 60 min. After being dried in a fume hood for 12 hours, the precursor hollow fibers were further dried under vacuum at 75°C for 12 hours.

Fabrication of polymer precursor dense films

Aramid dense films were fabricated by knife casting following a procedure described in our previous work (*17*). A polymer casting solution was prepared by dissolving dried aramid powders (16 wt %) in *N*,*N*-dimethylacetamide. The polymer solution was cast onto a borosilicate glass plate using a casting knife with 0.7-mm clearance. The nascent polymer film was heated in a convection oven at 120°C for 12 hours for solvent evaporation. The film was then soaked in methanol at room temperature for 12 hours to further remove the residual solvent. After being dried in a fume hood for 12 hours, the film was further dried under vacuum at 210°C for 24 hours.

Fabrication of CMS membranes

CMS hollow fiber membranes and CMS dense film membranes were fabricated by pyrolysis in a 24-inch (60.96 cm) pyrolysis tube furnace (MTI Corporation, Richmond, CA). CMS hollow fiber membranes were used for membrane permeation measurements, and CMS dense film membranes were used only for characterizations. The precursor hollow fibers or dense films were placed on a stainless-steel mesh plate (McMaster Carr, Robbinsville, NJ) and loaded into a quartz tube (MTI Corporation, Richmond, CA) before being placed in the pyrolysis furnace. Ultrahigh purity argon was flown in the quartz tube at 0.2 liter/min using a digital mass flow controller (MTI Corporation, Richmond, CA). The oxygen level inside the quartz tube was kept no higher than 5 parts per million, which was measured by an oxygen sensor (Cambridge Sensotec, Saint Ives, UK). The pyrolysis heating protocol consisted of the following: (i) room temperature to 250°C, 13.3°C/min; (ii) 250° to 1035°C, 3.85°C/min; (iii) 1035° to 1050°C, 0.25°C/min; (iv) dwelling at 1050°C for 2 hours; (v) natural cooling down to room temperature.

Membrane permeation measurements

CMS hollow fiber membrane modules (length, 35 cm) were constructed using stainless steel Swagelok tubings and fittings following procedures described in the literature (*35*). Two CMS hollow fiber membrane modules were used for permeation measurements, with each module comprising at least four CMS hollow fiber membranes made from separate batches of pyrolysis. A high-temperature epoxy resin (Duralco 4525; maximum temperature, 260°C) was used for sealing. Single-gas permeation measurements of H_2 and CO_2 were carried out using the constant volume-variable pressure method at 250° to 400°C. The hollow fiber membrane module was externally connected to the membrane permeation setup, with a single-zone (heating zone length, 20.3 cm) electric furnace (MTI Corporation, Richmond, CA) used to provide heating for the membrane module (fig. S11). The feed stream was introduced to the hollow fiber module shell side, and the permeate steam was withdrawn from the hollow fiber module bore (i.e., lumen) side. The epoxy ends of the CMS hollow fiber membrane modules were kept outside the furnace heating zone and were at room temperature during permeation measurements. The upstream and downstream sides of the membrane were evacuated for a minimum of 12 hours before introducing the feed. The permeation plots (i.e., rise in downstream

Downloaded from https://www.science.org on August 28, 2026

pressure with time) were recorded in LabVIEW (National Instruments, Austin, TX) and used to calculate the permeation flux. The time lags of CO_2 permeation plots are shown in fig. S2. Time lags cannot be reliably determined from H_2 permeation plots because of fast diffusion.

Mixed-gas H_2/CO_2 permeation measurements were carried out using the constant volume-variable pressure method with H_2/CO_2 mixture feeds. The experimental setup was similar to the one used for single-gas permeation measurements, except that a retentate stream was withdrawn from the hollow fiber module shell side so that the stage cut (the ratio of permeate molar flow rate to retentate molar flow rate) was kept below 1% to avoid the change in feed composition. The upstream and downstream sides of the membrane were evacuated for a minimum of 12 hours before introducing the feed. The permeation plots were recorded in LabVIEW and used to calculate the permeation flux. The composition of the permeate stream was measured using an Agilent 8890 gas chromatograph (Agilent Technologies, Santa Clara, CA). Gas chromatography injections were continuously taken until the membrane permeate composition was stabilized. Table S5 shows an example calculation of flux, permeance, permeability, and selectivity from mixed-gas H_2/CO_2 permeation measurements.

Material characterizations

Scanning electron microscopy was done using a Tescan XEIA3 scanning electron microscope (Tescan, Warrendale, PA). WAXD patterns of CMS dense films were recorded using a Bruker D8 Advance Lynx powder diffractometer (LynxEye PSD detector, sealed tube, Cu Kα radiation with Ni β-filter). Raman spectroscopy was performed in the CMS dense films using the H-J-Y LabRam ARAMIS Confocal Raman Microscope equipped with a 532-nm laser. XPS was performed in the CMS dense films using the Kratos AXIS Supra$^+$ spectrometer. Determination of elemental composition and peak fitting of the C1s, N1s, and O1s spectral scans were done in CasaXPS software. CO_2 physisorption (273.15 K) and H_2 physisorption (77 K) were performed in the CMS dense films by an ASAP 2020Plus physisorption analyzer (Micromeritics, Norcross, GA). CMS dense films were degassed at 120°C for 12 hours before collection of physisorption isotherms. A density functional theory model (CO_2, 273.15 K, carbon slit pores) was used to obtain the CMS pore size distribution using the CO_2 physisorption isotherms measured at 273.15 K. A density functional theory model (H_2, 77 K, carbon slit pores) was used to obtain the CMS pore size distribution using the H_2 physisorption isotherms measured at 77 K.

Supplementary Materials

This PDF file includes:

Supplementary Text
Figs. S1 to S11
Tables S1 to S5
References

REFERENCES AND NOTES

1. A. Boretti, B. K. Banik, Advances in hydrogen production from natural gas reforming. *Adv. Energy Sustainability Res.* **2**, 2100097 (2021).
2. N. W. Ockwig, T. M. Nenoff, Membranes for hydrogen separation. *Chem. Rev.* **107**, 4078–4110 (2007).
3. F. Dawood, M. Anda, G. M. Shafiullah, Hydrogen production for energy: An overview. *Int. J. Hydrogen Energy* **45**, 3847–3869 (2020).
4. M. Melaina, M. Penev, D. Heimiller, "Resource assessment for hydrogen production: Hydrogen production potential from fossil and renewable energy resources" (NREL/TP-5400-55626, NREL, 2013).
5. R. W. Baker, B. T. Low, Gas separation membrane materials: A perspective. *Macromolecules* **47**, 6999–7013 (2014).
6. D. F. Sanders, Z. P. Smith, R. Guo, L. M. Robeson, J. E. McGrath, D. R. Paul, B. D. Freeman, Energy-efficient polymeric gas separation membranes for a sustainable future: A review. *Polymer* **54**, 4729–4761 (2013).
7. Y. Han, W. S. W. Ho, Polymeric membranes for CO_2 separation and capture. *J. Membr. Sci.* **628**, 119244 (2021).
8. L. Liu, D. Liu, C. Zhang, High-temperature hydrogen/propane separations in asymmetric carbon molecular sieve hollow fiber membranes. *J. Membr. Sci.* **642**, 119978 (2022).
9. C. Zhang, G. B. Wenz, P. J. Williams, J. M. Mayne, G. Liu, W. J. Koros, Purification of aggressive supercritical natural gas using carbon molecular sieve hollow fiber membranes. *Ind. Eng. Chem. Res.* **56**, 10482–10490 (2017).
10. Z. Liu, W. Qiu, W. Quan, W. J. Koros, Advanced carbon molecular sieve membranes derived from molecularly engineered cross-linkable copolyimide for gas separations. *Nat. Mater.* **22**, 109–116 (2023).
11. T. Araújo, M. Andrade, G. Bernardo, A. Mendes, Stable cellulose-based carbon molecular sieve membranes with very high selectivities. *J. Membr. Sci.* **641**, 119852 (2022).
12. X. Ma, Y. S. Lin, X. Wei, J. Kniep, Ultrathin carbon molecular sieve membrane for propylene/propane separation. *AIChE J.* **62**, 491–499 (2016).
13. D.-Y. Koh, B. A. McCool, H. W. Deckman, R. P. Lively, Reverse osmosis molecular differentiation of organic liquids using carbon molecular sieve membranes. *Science* **353**, 804–807 (2016).
14. C. Zhang, R. Kumar, W. J. Koros, Ultra-thin skin carbon hollow fiber membranes for sustainable molecular separations. *AIChE J.* **65**, e16611 (2019).
15. K. Hazazi, Y. Wang, N. M. S. Bettahalli, X. Ma, Y. Xia, I. Pinnau, Catalytic arene-norbornene annulation (CANAL) ladder polymer derived carbon membranes with unparalleled hydrogen/carbon dioxide size-sieving capability. *J. Membr. Sci.* **654**, 120548 (2022).
16. T. Merkel, "Novel polymer membrane process for pre-combustion CO2 capture from coal-fired syngas" (Membrane Technology and Research, Incorporated, 2011).
17. G. M. Iyer, C. Zhang, Precise hydrogen sieving by carbon molecular sieve membranes derived from solution-processable aromatic polyamides. *ACS Mater. Lett.* **5**, 243–248 (2023).
18. A. Garshasbi, H. Chen, M. Cao, S. Karagöz, R. J. Ciora, P. K. T. Liu, V. I. Manousiouthakis, T. T. Tsotsis, Membrane-based reactive separations for process intensification during power generation. *Catal. Today* **331**, 18–29 (2019).
19. L. Liu, A. Bhowmick, S. Cheng, B. H. Blazquez, Y. Pan, J. Zhang, Y. Zhang, Y. Shu, D. T. Tran, Y. Luo, M. Ierapetritou, C. Zhang, D. Liu, Alkane dehydrogenation in scalable and electrifiable carbon membrane reactor. *Cell Rep. Phys. Sci.* **4**, 101692 (2023).
20. M. Omidvar, H. Nguyen, H. Liang, C. M. Doherty, A. J. Hill, C. M. Stafford, X. Feng, M. T. Swihart, H. Lin, Unexpectedly strong size-sieving ability in carbonized polybenzimidazole for membrane H_2/CO_2 separation. *ACS Appl. Mater. Interfaces* **11**, 47365–47372 (2019).
21. L. Xu, M. Rungta, J. Hessler, W. Qiu, M. Brayden, M. Martinez, G. Barbay, W. J. Koros, Physical aging in carbon molecular sieve membranes. *Carbon* **80**, 155–166 (2014).
22. G. M. Iyer, C.-E. Ku, C. Zhang, Polyamide-imide copolymer-derived carbon molecular sieve membranes for efficient hydrogen/carbon dioxide separation. *Carbon* **216**, 118598 (2024).
23. L. Lei, F. Pan, A. Lindbråthen, X. Zhang, M. Hillestad, Y. Nie, L. Bai, X. He, M. D. Guiver, Carbon hollow fiber membranes for a molecular sieve with precise-cutoff ultramicropores for superior hydrogen separation. *Nat. Commun.* **12**, 268 (2021).
24. M. Shan, X. Liu, X. Wang, I. Yarulina, B. Seoane, F. Kapteijn, J. Gascon, Facile manufacture of porous organic framework membranes for precombustion CO_2 capture. *Sci. Adv.* **4**, eaau1698 (2018).
25. H. Li, Z. Song, X. Zhang, Y. Huang, S. Li, Y. Mao, H. J. Ploehn, Y. Bao, M. Yu, Ultrathin, molecular-sieving graphene oxide membranes for selective hydrogen separation. *Science* **342**, 95–98 (2013).
26. C. Zhang, W. J. Koros, Ultraselective carbon molecular sieve membranes with tailored synergistic sorption selective properties. *Adv. Mater.* **29**, 1701631 (2017).
27. W. Qiu, J. E. Leisen, Z. Liu, W. Quan, W. J. Koros, Key features of polyimide-derived carbon molecular sieves. *Angew. Chem. Int. Ed.* **60**, 22322–22331 (2021).
28. J. Jagiello, A. Ansón, M. T. Martínez, DFT-based prediction of high-pressure H_2 adsorption on porous carbons at ambient temperatures from low-pressure adsorption data measured at 77 K. *J. Phys. Chem. B* **110**, 4531–4534 (2006).
29. R. W. Baker, K. Lokhandwala, Natural gas processing with membranes: An overview. *Ind. Eng. Chem. Res.* **47**, 2109–2121 (2008).
30. Z. Ali, F. Pacheco, E. Litwiller, Y. Wang, Y. Han, I. Pinnau, Ultra-selective defect-free interfacially polymerized molecular sieve thin-film composite membranes for H_2 purification. *J. Mater. Chem. A* **6**, 30–35 (2018).
31. M. Luberti, H. Ahn, Review of polybed pressure swing adsorption for hydrogen purification. *Int. J. Hydrogen Energy* **47**, 10911–10933 (2022).

Downloaded from https://www.science.org on August 28, 2026

32. T. C. Merkel, H. Lin, X. Wei, R. Baker, Power plant post-combustion carbon dioxide capture: An opportunity for membranes. *J. Membr. Sci.* **359**, 126–139 (2010).
33. M. Y. Jeon, D. Kim, P. Kumar, P. S. Lee, N. Rangnekar, P. Bai, M. Shete, B. Elyassi, H. S. Lee, K. Narasimharao, S. N. Basahel, S. Al-Thabaiti, W. Xu, H. J. Cho, E. O. Fetisov, R. Thyagarajan, R. F. DeJaco, W. Fan, K. A. Mkhoyan, J. I. Siepmann, M. Tsapatsis, Ultra-selective high-flux membranes from directly synthesized zeolite nanosheets. *Nature* **543**, 690–694 (2017).
34. M. R. Kosuri, W. J. Koros, Defect-free asymmetric hollow fiber membranes from Torlon®, a polyamide–imide polymer, for high-pressure CO_2 separations. *J. Membr. Sci.* **320**, 65–72 (2008).
35. D. Q. Vu, W. J. Koros, S. J. Miller, High pressure CO_2/CH_4 separation using carbon molecular sieve hollow fiber membranes. *Ind. Eng. Chem. Res.* **41**, 367–380 (2002).
36. M. Dakhchoune, L. F. Villalobos, R. Semino, L. Liu, M. Rezaei, P. Schouwink, C. E. Avalos, P. Baade, V. Wood, Y. Han, M. Ceriotti, K. V. Agrawal, Gas-sieving zeolitic membranes fabricated by condensation of precursor nanosheets. *Nat. Mater.* **20**, 362–369 (2021).
37. M. Yu, H. H. Funke, R. D. Noble, J. L. Falconer, H_2 separation using defect-free, inorganic composite membranes. *J. Am. Chem. Soc.* **133**, 1748–1750 (2011).
38. A. Huang, Q. Liu, N. Wang, Y. Zhu, J. Caro, Bicontinuous zeolitic imidazolate framework ZIF-8@GO membrane with enhanced hydrogen selectivity. *J. Am. Chem. Soc.* **136**, 14686–14689 (2014).
39. Y. Ying, M. Tong, S. Ning, S. K. Ravi, S. B. Peh, S. C. Tan, S. J. Pennycook, D. Zhao, Ultrathin two-dimensional membranes assembled by ionic covalent organic nanosheets with reduced apertures for gas separation. *J. Am. Chem. Soc.* **142**, 4472–4480 (2020).
40. R. M. de Vos, H. Verweij, High-selectivity, high-flux silica membranes for gas separation. *Science* **279**, 1710–1711 (1998).
41. Y. Peng, Y. Li, Y. Ban, W. Yang, Two-dimensional metal–organic framework nanosheets for membrane-based gas separation. *Angew. Chem. Int. Ed.* **56**, 9757–9761 (2017).
42. Z. Kang, M. Xue, L. Fan, L. Huang, L. Guo, G. Wei, B. Chen, S. Qiu, Highly selective sieving of small gas molecules by using an ultra-microporous metal–organic framework membrane. *Energ. Environ. Sci.* **7**, 4053–4060 (2014).
43. L. Hu, V. T. Bui, A. Krishnamurthy, S. Fan, W. Guo, S. Pal, X. Chen, G. Zhang, Y. Ding, R. P. Singh, M. Lupion, H. Lin, Tailoring sub-3.3 Å ultramicropores in advanced carbon molecular sieve membranes for blue hydrogen production. *Sci. Adv.* **8**, eabl8160 (2022).

Acknowledgments: We thank K. Gaskell from the University of Maryland Surface Analysis Center for helping with XPS measurements. We also acknowledge the support of the Maryland NanoCenter and the AIMLab. **Funding:** This work was supported by the Office of Energy Efficiency and Renewable Energy of the US Department of Energy (award no. DE-EE0010313) and the US National Science Foundation (award no. NSF-CBET 2044794).
Author contributions: Conceptualization: C.Z. Methodology: C.Z. and G.M.I. Investigation: G.M.I. and C.-E.K. Visualization: C.Z., G.M.I., and C.-E.K. Funding acquisition: C.Z. Project administration: C.Z. Supervision: C.Z. Writing—original draft: C.Z. Writing—review and editing: G.M.I. and C.-E.K. **Competing interests:** C.Z. and G.M.I. are inventors on a patent application (US20240342664A1) submitted by the University of Maryland on 24 October 2023. The other author declares no competing interests. **Data and materials availability:** All data needed to evaluate the conclusions in the paper are present in the paper and/or the Supplementary Materials.

Submitted 14 October 2024
Accepted 30 April 2025
Published 4 June 2025
10.1126/sciadv.adt7512

Downloaded from https://www.science.org on August 28, 2026

ScienceAdvances

Hyperselective carbon membranes for precise high-temperature H_2 and CO_2 separation

Gaurav M. Iyer, Ching-En Ku, and Chen Zhang

Sci. Adv. **11** (23), eadt7512. DOI: 10.1126/sciadv.adt7512

View the article online
https://www.science.org/doi/10.1126/sciadv.adt7512
Permissions
https://www.science.org/help/reprints-and-permissions

Downloaded from https://www.science.org on August 28, 2026

Use of this article is subject to the Terms of service

Science Advances (ISSN 2375-2548) is published by the American Association for the Advancement of Science. 1200 New York Avenue NW, Washington, DC 20005. The title *Science Advances* is a registered trademark of AAAS.

Copyright © 2025 The Authors, some rights reserved; exclusive licensee American Association for the Advancement of Science. No claim to original U.S. Government Works. Distributed under a Creative Commons Attribution NonCommercial License 4.0 (CC BY-NC).